

## Supplementary Information

### Liquid-liquid critical point in supercooled silicon

Vishwas V Vasisht, Shibu Saw, Srikanth Sastry

Here we present additional details of simulations that are performed to construct the phase diagram of liquid silicon. These include the estimation of the liquid-liquid coexistence line, the spinodal, the tensile limit loci, the lines of density maxima and minima, and the lines of compressibility maxima and minima.

1. **Line of Liquid-Liquid Coexistence:** The coexistence line is calculated from isobars generated using NPT MD simulations (with system size of 512 particles). We find sudden jumps in density for small changes in temperature, which indicate the location of the first order phase transition.

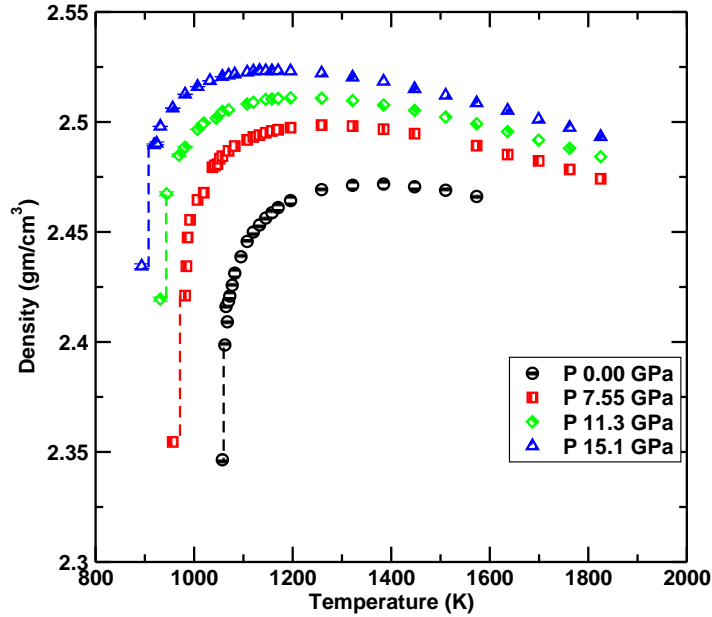


FIG. 1: Density *vs.* temperature isobars showing discontinuous changes in density for small changes in temperature at constant pressure. These jumps are used to locate the temperature at which a first order transition occurs at the studied pressures.

2. **Liquid-Gas coexistence line:** To obtain the L-G coexistence line we perform Gibbs-Ensemble Monte Carlo - GEMC (*see Understanding Molecular Simulation by D. Frenkel and B. Smit*) simulations (with 2000 particles). In a GEMC simulation

we obtain, at coexistence, liquid and gas phases in two different simulation boxes. When phase equilibrium is achieved, the pressure, the temperature and the chemical potential of both the simulation boxes will be the same. At each temperature we obtain the coexistence pressure to construct the liquid-gas coexistence line.

3. **Spinodal line:** The spinodal point is defined by the condition  $(\partial P/\partial V)_T = 0$ . In Fig. 2 we show high temperature spinodal isotherms ( $T > 2200K$ ). These isotherms are obtained from constant volume temperature (NVT) MD simulations, with system size of 512 particles. At each state point we perform simulations for around 7 ns to 20 ns.

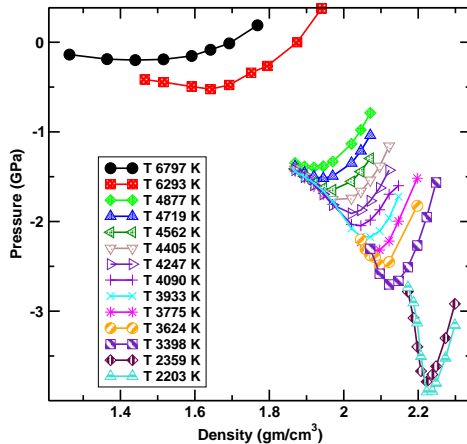


FIG. 2: The plot of pressure *vs.* density showing high temperature isotherms. The isotherms go through minima which are identified as spinodal points.

For  $T < 2200$  K, we find cavitation in the NVT simulations before minima along isotherms are reached, due to which we observe a drastic increase in the pressure. In an attempt to circumvent this problem, we perform restricted ensemble Monte Carlo (REMC) simulations. In an REMC simulation, arbitrary bounds were imposed on the magnitude of the allowed density fluctuations. This is accomplished by dividing the simulation box into a number of equal sub-cells and a constraint is imposed on the number of particles in each of these sub-cells. If the number of sub-cells is  $n$ , the instantaneous number of particles ( $N_i$ ) in each sub-cell  $i$  is constrained to satisfy  $(\langle N \rangle - \delta N) \leq N_i \leq (\langle N \rangle + \delta N)$ , where  $\langle N \rangle = (N/n)$  is the average number of particles in each sub-cell and  $\delta N$  is the maximum allowed deviation from the average

value. The value of  $\delta N$  should be greater than unconstrained fluctuation of particles which is given by  $\Delta N = [\langle N \rangle k_B T K_T \rho]^{1/2}$ . Here  $k_B$  is the Boltzmann constant,  $K_T$  is the compressibility at temperature  $T$  and density  $\rho$ . We perform REMC simulations in a 1500 particles system by dividing the system into 4x4x4 and 5x5x5 sub-cells. The value of  $\Delta N$  is estimated at different state points based on NVT simulations and  $\delta N$  is chosen to be three times  $\Delta N$ . The total simulation length in each case is 5 million MC cycles. However, we find that even in these REMC simulations, the system cavitates, with the formation of voids across sub-cell boundaries (with each sub-cell satisfying the applied constraint on number of particles). Hence we estimate the spinodal at these state points from a quadratic extrapolation of the isotherms. We fit the data points obtained from REMC simulations with a quadratic function ( $p_0 + a1 * (\rho - \rho_0) + a2 * (\rho - \rho_0)^2$ ), where  $p_0$  and  $\rho_0$  are the spinodal pressure and density values. The data and the fits are shown in Fig. 3.

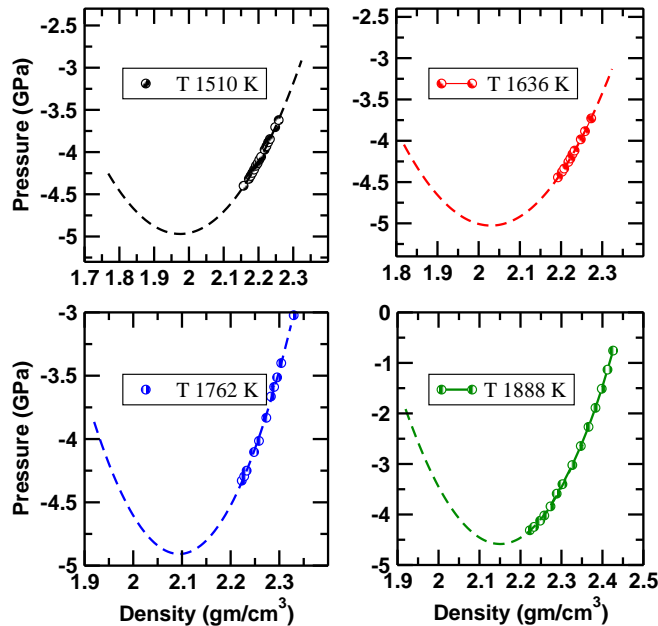


FIG. 3: The plot of pressure *vs.* density for low temperature ( $T < 2200K$ ) isotherms. The dashed line indicate the quadratic ( $p_0 + a1 * (\rho - \rho_0) + a2 * (\rho - \rho_0)^2$ ) extrapolation.

4. **Tensile limit line:** The locus of maximum tensile stress (negative pressure) a system can withstand before it fails defines the tensile limit line. The protocol used to obtain the tensile limit is as follows. At a given temperature we first equilibrate the system

at a high pressure (for  $T < 1510$  K we equilibrate at  $P = -2.26$  GPa and for  $T > 1510$  K at  $P = 0$  GPa, by performing NPT MD simulation for 4 ns. All the simulations are performed with 512 particles). We then apply a tensile pressure to this equilibrated sample that increases at a specified rate. We perform simulations at two different constant rates of change of tensile pressure. When the system reaches its limit of tensile strength, the system's density decreases drastically towards zero. In Fig. 4, and Fig. 5 we show the applied pressure against the measured density for a range of temperatures, from which we obtain the tensile limit line. At faster stretching rate (10 MPa/ps) we find tensile limits that are consistent with the spinodal estimates described above. For slow stretching rate (0.1 MPa/ps) we find that the system cavitates at higher pressure values. We have also performed simulations at intermediate rate, 1.0 MPa/ps (not reported in this letter) and we find that the estimated tensile limit line lies in between the estimates obtained from the fast and slow stretching rates. For slow stretching rate we perform simulations for around 70 ns. These simulations are performed with the LAMMPS package.

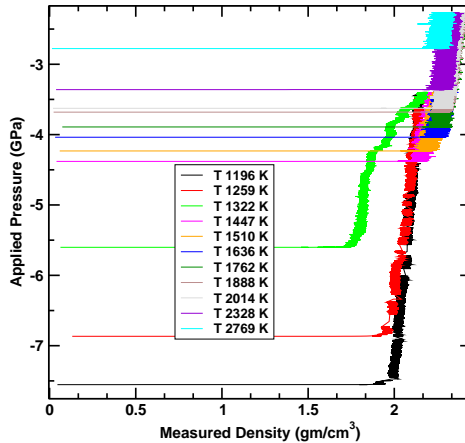


FIG. 4: The plot of applied pressure against measured density for different isotherms. The stretching rate is 0.1 MPa/ps

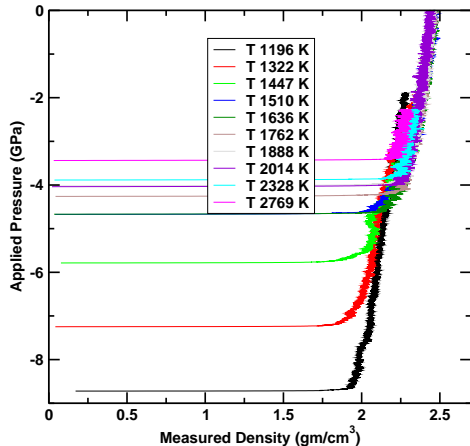


FIG. 5: The plot of applied pressure against measured density for different isotherms. The stretching rate is 10.0 MPa/ps

5. **Temperature of maximum density:** The temperature of maximum density is the locus of isobaric maxima of density  $\rho$  vs.  $T$  ( $(\partial\rho/\partial T)_P = 0$ ) or the locus of isochoric minima of pressure  $P$  vs.  $T$  ( $(\partial P/\partial T)_V = 0$ ). For pressure values above  $P = -3.80$  GPa, we obtain the TMD from NPT MD simulations to locate isobaric maxima of density. But below  $P = -3.80$ , since cavitation is a possibility in NPT simulations, we perform NVT MD simulations to locate isochoric minima of pressure. The TMD obtained from density maxima along isobars and pressure minima along isochores are shown in Fig. 6 and Fig. 7 respectively. The simulation length for these state points is around 10 ns (more than  $100\tau$  where  $\tau$  is the relaxation time) and the system size is 512 particles.
6. **Temperature of minimum density:** TMinD is locus of density minima points, crossing which, the system returns to normal behaviour. Finding the TMinD line in supercooled silicon is challenging since we must simulate the system deep inside the supercooled region of the phase diagram (where crystallisation, slow equilibration and cavitation pose hurdles to obtaining equilibrated data). In order to obtain equilibrated data we employ NPT parallel tempering Monte Carlo simulations (*see Understanding Molecular Simulation by D. Frenkel and B. Smit*), in which we perform swaps between replicas at different T and P. The paths chosen to perform parallel tempering are shown in the Fig. 8. We perform simulations, with a system size of 512 particles, up

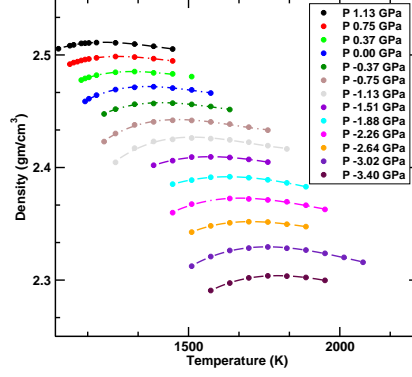


FIG. 6: The plot of density against temperature for different isobars. The maxima obtained at each isobar constitutes the TMD line.

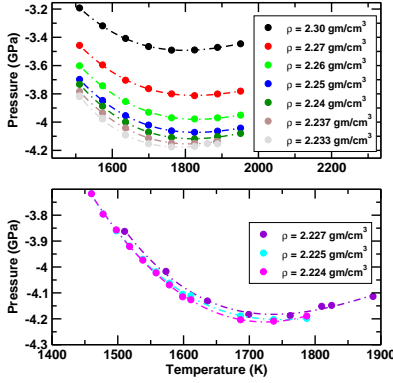


FIG. 7: (top panel) The plot of pressure against temperature for different isochores. The minima obtained at each isochores constitutes the TMD line. In the bottom panel we show last three isochores at which we could perform NVT simulations. Below these densities, the system cavitates before going through a pressure minimum.

to 60 million MC cycles. To check the equilibration of the system using the following tests: We ensure that each replica gets swapped up and down in temperature  $T$  atleast 100 times. We calculate the mean squared displacement (MSD) for each replica and ascertain that every particle in the system has moved atleast  $5\sigma$ .

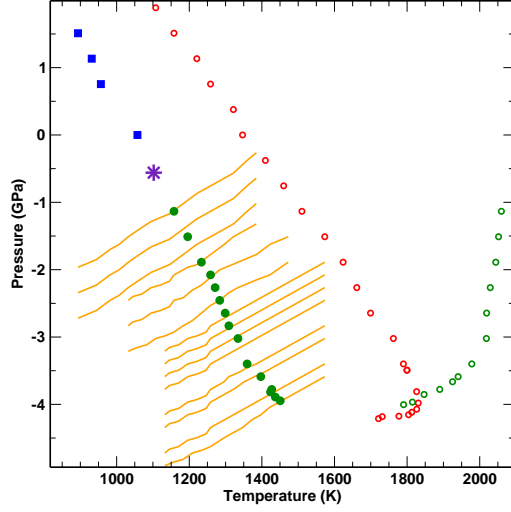


FIG. 8: The phase diagram showing the paths chosen to perform NPT-PT simulations. The orange lines are the paths along which NPT-PT simulations are performed. The green points indicate compressibility extrema, the red points the density maxima, the purple points the liquid-liquid coexistence line, and the star indicates the location of the critical point.

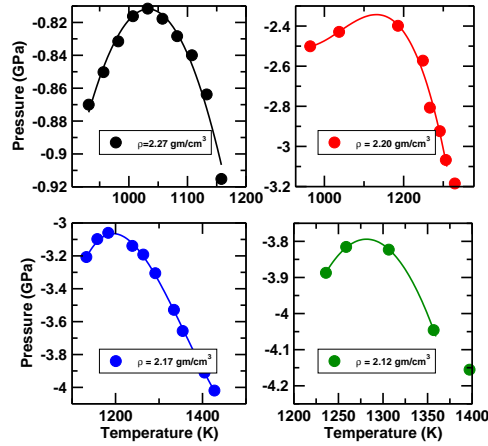


FIG. 9: Pressure *vs.* temperature for different isochores. The maxima obtained at each isochore constitute the TMinD line.

7. **Temperature of minimum compressibility (TMinC):** We perform NPT MD simulations (with 512 particles) to obtain TMinC points. The relaxation time at these state points are of the order of a few ns (or 10 to 30 million MD steps). We face the issue of cavitation below  $-3.80$  GPa. In this region of the phase diagram we have performed simulations for a minimum of 10 independent samples to construct the equation of state (EOS), from which we obtain the compressibility by taking the derivative of the pressure with respect to density.

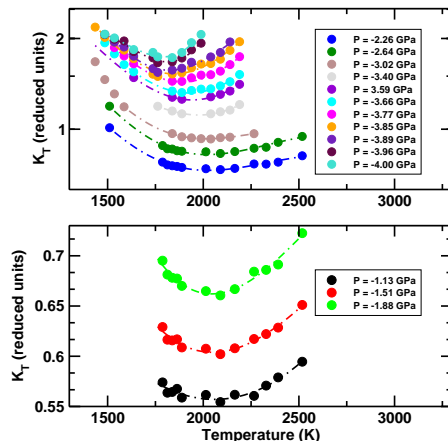


FIG. 10: Compressibility *vs.* temperature for different isobars. The minima obtained along isobars constitute the TMinC line.

8. **Temperature of maximum compressibility:** The high pressure ( $P > -2$  GPa) compressibility maxima ( $K_T^{max}$ ) are shown in the manuscript (Fig. 2). Compressibility data from which  $K_T^{max}$  are obtained for  $P < -2$  GPa are shown in the Fig. 11. We find that as the system crosses the  $K_T^{max}$  line from high T to low T (at a chosen pressure value), the relaxation times increases from picoseconds to tens of nanoseconds. Nearing the compressibility maxima we also find that many samples crystallise. The  $K_T$  values shown in the Fig. 11 are calculated from both volume fluctuations measured in NPT MD simulations and from derivatives of pressure from NVT MD simulations. For pressure value below  $-3.90$  GPa, the system cavitates easily and hence we cannot evaluate the location of  $K_T^{max}$  in this region of the phase diagram.

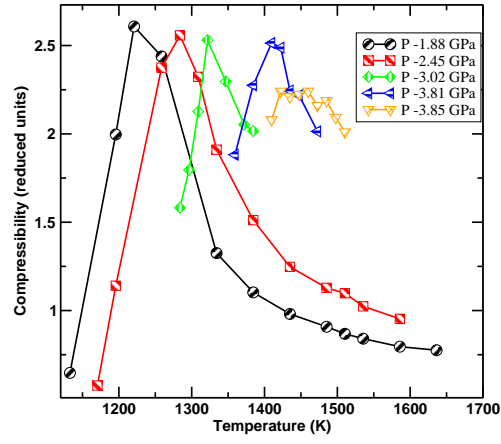


FIG. 11: Compressibility *vs.* temperature for different isobars. The maxima obtained along isobars constitute the TMC line.

# Liquid-liquid critical point in supercooled silicon

Vishwas V Vasisht, Shibu Saw, and Srikanth Sastry\*

*Jawaharlal Nehru Centre for Advanced Scientific Research, Bangalore 560064, India.*

arXiv:1103.3473v1 [cond-mat.stat-mech] 17 Mar 2011

---

\* Corresponding Author: [sastry@jncasr.ac.in](mailto:sastry@jncasr.ac.in)

A novel liquid-liquid phase transition has been proposed and investigated in a wide variety of pure substances recently, including water, silica (major components of the earth’s crust), the technologically important element silicon, and others marked by energetically stabilized tetrahedral local geometries. From computer simulations using a classical empirical potential (the Stillinger-Weber potential), Sastry and Angell [1] demonstrated a first order liquid-liquid transition in supercooled silicon, supported by further experimental and simulation studies subsequently. Here, we report evidence for a critical end point to the liquid-liquid phase transition at negative pressures, from computer simulations using the SW potential. Compressibilities, evaluated from the equation of state and fluctuations in constant pressure-temperature simulations exhibit a growing maximum upon lowering temperature below  $1500K$  and isotherms exhibit density discontinuities below  $1120K$ , at negative pressure. Below  $1120K$ , isotherms obtained from constant volume-temperature simulations exhibit non-monotonic, van der Waals-like behavior signaling a first order transition. We identify  $T_c \sim 1120 \pm 12K$ ,  $P_c \sim -0.60 \pm 0.15GPa$  as the critical temperature and pressure for the liquid-liquid critical point. The structure of the liquid changes dramatically upon decreasing the temperature and pressure. Diffusivities vary over 4 orders of magnitude, and exhibit anomalous pressure dependence near the critical point. A strong relationship between local geometry quantified by the coordination number, and diffusivity, is seen, suggesting that atomic mobility in both low and high density liquids can usefully be analyzed in terms of defects in the tetrahedral network structure. We have constructed the phase diagram of supercooled silicon. We identify the lines of compressibility, density extrema (maxima and minima) and the spinodal which reveal the interconnection between thermodynamic anomalies and the phase behaviour of the system as suggested in previous works [2–9].

The possibility of a phase transition between two forms of the liquid phase in some pure substances has attracted considerable interest and research activity in recent years [1–3, 5, 7–9]. Among the substances investigated are water [5, 7, 8], silica [9] and silicon [1, 10–16], germanium, carbon and hydrogen – these substances together form a very significant component of our natural world, living organisms, and technology. A phenomenon common

to these is therefore of wide general interest. As illustrated in [17], further, liquid-liquid transitions offer an avenue for interesting applications by exploiting the different properties of distinct liquid phases.

Although the liquid-liquid transition was discussed in the context of silicon [10] somewhat earlier, the considerable current interest stems from various proposals for understanding the anomalies of water [3, 5–7, 18–20]. These scenarios have alternately invoked the approach to a spinodal[3], a liquid-liquid critical point[5, 7], general thermodynamic constraints without the presence of any singular behavior[6], and the presence of a transition without a critical end point[20], in rationalizing experimentally observed behavior. In spite of substantial investigations, a general consensus is yet lacking on the interpretation of observed behavior [18, 20]. In particular, recent experiments on confined water [19] and issues surrounding their interpretation [20] indicate the need to ascertain the existence of a critical end point even when sufficient evidence exists for a liquid-liquid transition.

The possibility of a transition in supercooled silicon was suggested [11] based on estimates of excess Gibbs free energies of amorphous and liquid silicon, implying a “amorphous-liquid” phase transition near 1,450 K (below the freezing point of the liquid, 1,685 K). Clear evidence of a transition between two liquids in the supercooled region was shown in [1] from molecular dynamics simulations using Stillinger-Weber (SW) potential [21]. A first order transition at zero pressure was found at  $T = 1060$  K, substantially below the experimental estimate. However, recent electrostatic levitation experiments performed down to  $T = 1382$  K do not find evidence for a transition [22]. Apart from the uncertainties in the experimental value, such a difference may be expected to arise from the neglect in the empirical potential of significant changes in the electronic structure associated with structural change [15, 16], though first principles simulations [16] appear to confirm the transition temperature obtained from the classical simulations. The exact location of the transition must thus be viewed as tentative at present.

In the present work, we use molecular dynamics (MD) simulations using the SW potential for silicon to locate the liquid-liquid critical point, and show that it lies at negative pressures. We perform constant pressure, temperature (NPT) and constant volume, temperature (NVT) simulations of 512 atoms, using protocols described in *Methods*. Pressure *vs.* density isotherms generated in the temperature range of 1070K to 1510K, and the pressure range of  $-3.8$  GPa to  $+3.8$  GPa using NPT simulations are shown in Fig. 1 (top panel).

The isotherms for temperatures above  $T = 1133K$  are continuous, but develop an inflection below  $T = 1259K$  which becomes more pronounced as temperature is lowered. The compressibility develops a maximum in this temperature range, which grows as the temperature is lowered. Below  $T = 1108K$ , careful constant pressure simulations always result in a jump in the density as pressure is varied, suggesting a first order transition. To verify this further, we perform NVT simulations for  $T = 1108K, 1082K, 1070K$  in the density range where NPT simulations show a jump. These results are shown in the bottom panel of Fig. 1. We find that at these temperatures, the isotherms are non-monotonic. Such non-monotonicity in simulations arises from metastability on the one hand, and on the other hand, incomplete phase separation owing to finite sample sizes in the unstable region, and constitutes a clear indication of a first order transition. Thus, our equation of state data show isotherms with growing compressibility maxima as temperature is decreased (above  $T = 1133K$ ) and first order transitions (below  $T = 1108K$ ) between two liquids, the high density liquid (HDL) and the low density liquid (LDL). We thus deduce that the critical end point to be located between these temperatures. Inspection of Fig. 1 (bottom panel) also makes it clear that the critical pressure must be negative. Based on the above data at the temperatures simulated, we estimate the location of the critical point to be at  $T_c \sim 1120 \pm 12K$ ,  $P_c \sim -0.6 \pm .15GPa$ . A more precise estimation of critical parameters require analysis, including finite size scaling, which is beyond the scope of the present paper but are being pursued as extensions of the present work.

Approaching the critical point from above leads to increased density fluctuations. In addition to evaluating the compressibility from the equation of state (EOS), we also calculate it directly from density fluctuations. These are shown in Fig. 2 for temperatures above  $T = 1133K$  which show good agreement with EOS estimates for the high density liquid (HDL), but poorer agreement for the low density liquid (LDL). The high crystallization rates observed near and at lower pressures than the compressibility maxima hamper improved sampling (however we report results only from equilibrated runs). The influence of fluctuations and local structure (see below) on nucleation rates [23, 24] is an interesting issue that is presently being investigated.

Next we describe briefly the temperature and density dependence of diffusivities  $D$  and average coordination number  $N_n$ , which captures important information regarding structural change.  $N_n$ , the *number of neighbors* of an atom is calculated by integrating the pair

correlation function up to its first minimum. In Fig. 3 (top panel)  $N_n$  is shown as a function of pressure. At high temperatures and pressures,  $N_n$  is about 5, and decreases as temperature and pressure are lowered, showing discontinuous change below 1133K, and values close to the tetrahedral value of 4 ( $\sim 4.1$ ) in the LDL, similar to the observation at zero pressure in [1].

Diffusivities *vs.* pressure for the studied temperatures are shown in (Fig. 3 - bottom panel), which increase with pressure for all the temperatures shown, in analogy with the well known anomaly in water. Like the coordination number, diffusivities show a discontinuity below  $T = 1133K$ , with a jump of roughly two orders of magnitude from HDL to LDL. The diffusivities span a range of over four orders of magnitude.

In Fig. 4, we show the diffusivities  $D$  plotted against coordination number  $N_n$ . Except at the highest temperature studied, we find the dependence of  $D$  on  $N_n$  to be remarkably similar irrespective of temperature, including those below the critical temperature. The mobility of atoms therefore is very strongly determined by the local structure. This observation is consistent with previous analysis of the role of “bifurcated bonds” or the “fifth neighbor” in determining molecular mobility in water [26]. It is tempting to speculate that apart from trivial thermal effects, a universal dependence exists of atomic mobility on the average number of neighbors in excess of the tetrahedral value of 4. To test this possibility, we show in the inset of Fig. 4 a scaled plot of  $D$ , by normalizing to its value at a fixed  $N_n$  in the HDL phase for all temperatures. The data collapse is indeed remarkable and the resulting master curve can be well fit to a Vogel-Fulcher-Tammann (VFT) form,  $D(n) = D_0 \exp(-\frac{A}{n-n_0})$  with  $n_0 = 3.86$ . Further analysis of this interesting observation is in progress.

Previous studies of the phase behavior of water and other liquids exhibiting density anomalies have analyzed the interplay of various loci of extremal behavior, namely the spinodal, lines of density maxima (TMD) [3], density minima (TMinD) [27], compressibility minima (TMinC) and maxima (TMC). To obtain a comprehensive picture of the phase behavior of liquid silicon, we have evaluated these loci, employing in addition to the MD simulations, parallel tempering (PT) and restricted ensemble (REMC) Monte Carlo simulations [28] for locating the spinodal (details and data are provided in the supplementary information (SI)) at low temperatures. As shown in Figure 5, the spinodal we estimate is monotonic in pressure *vs.* temperature  $T$ , *ie* not “reentrant” as predicted to be the case [3] if it intersects with the TMD. The TMD, however, changes slope upon intersection with

the TMinC, as analyzed in [6]. Evaluating the relevant equation of state data is particularly challenging in this case as the TMD approaches the spinodal very closely, while not intersecting it. From available data, it appears that the TMinC will join smoothly with the TMC (line of compressibility maxima) that emanates from the liquid-liquid critical point. Interestingly, we find from PT simulations below the critical temperature and pressure that there exists also a line of density minima, very recently observed in the case of water in experiments and computer simulations [27]. The TMD and the TMinD appear to smoothly join with each other, as required by thermodynamic consistency.

At low temperatures  $T$  ( $1440K < T < 2000K$ ), even REMC simulations (which restrict density fluctuations) cavitate at sufficiently low pressure. In these cases, we estimate the spinodal by a quadratic extrapolation of the isotherms. As a further check on our spinodal estimate, we perform simulations to obtain tensile limits by increasing the tensile pressure on the simulation cell at constant rates, for two different rates (0.1 and 10.0 MPa/ps). For the faster rate, we find tensile limits that are consistent with the spinodal estimates we have, while for the slower rate, the system cavitates at higher pressures, remaining nevertheless monotonic *vs.* temperature. These simulations also extend our estimate of the spinodal to lower temperatures, and indicate a marked downturn of the spinodal pressure below the temperatures we have studied.

In conclusion, we have performed extensive molecular dynamics and Monte Carlo simulations of supercooled liquid silicon using the SW potential to find evidence for a negative pressure liquid-liquid critical point. We estimate the location of the critical point to be at  $T_c \sim 1120 \pm 12K$ ,  $P_c \sim -0.60 \pm 0.15GPa$ . We have computed the phase diagram of supercooled liquid silicon. We find no retracing of spinodal. The phase behaviour of silicon is similar to that observed in simulations of water and silica. The structure of the liquid changes dramatically in going from high temperatures and pressures to low temperatures and pressures. Diffusivities vary by more than 4 orders of magnitude, and exhibit anomalous pressure dependence. A strong relationship between local geometry quantified by the coordination number and diffusivity is seen, suggesting that atomic mobility in both low and high density liquids can usefully be analyzed in terms of defects in the tetrahedral network structure.

## Methods :

We perform Molecular Dynamics (MD), with a time step of 0.383 fs, with details as in [1],

but employing an efficient algorithm[29] for energy and force evaluations. NVT simulations employ the LAAMPS [30] parallelised MD package. PT and REMC Monte Carlo simulations are described in the SI.

In the HDL phase, a minimum of 3 to 6 independent samples are simulated for  $\sim 100$  relaxation times ( $\sim 10$  ns). In the LDL phase, crystallisation (monitored by energy jumps, mean square displacement (MSD) and pair correlation function) rates are high. We perform around 10 to 50 initial runs, each of 22 ns. Noncrystallizing samples (average of 5) were run up to 10 relaxation times when possible. In all LDL cases, simulations were carried out for times required for the MSD to reach  $1nm^2$  ( $5 \sigma^2$ , where  $\sigma$  is the atomic diameter) or for  $100ns$  (300 million MD steps), whichever is larger.

Equilibration is monitored by the MSD and the overlap function  $Q(t)$ , defined as  $Q(t) = \frac{1}{N} \sum_{i=1}^N w |\vec{r}_i(t_0) - \vec{r}_i(t_0 + t)|$ , where  $w(r) = 1$ , if  $r \leq 0.3\sigma$ , zero otherwise. We evaluate relaxation times ( $\tau$ ) by fitting  $Q(t)$  to a stretched exponential function. As an indication of its variation,  $\tau$  varies at  $P = 0GPa$  in the HDL from 0.3 ps ( $T = 1260$  K) to 0.01 ns ( $T = 1068$  K) and in LDL phase at  $T = 1060$  K, the  $\tau$  is around 30ns.

We calculate the compressibility  $K_T$  from the EOS using:

$$K_T = \frac{1}{\rho} \left[ \frac{\partial \rho}{\partial P} \right]_T.$$

Polynomial fits to isotherms are used in calculating the derivatives. We also calculate  $K_T$  from volume fluctuations (NPT simulations) using:

$$K_T = \frac{\langle V^2 \rangle - \langle V \rangle^2}{\langle V \rangle k_B T}.$$

The latter method is computationally very demanding, and the comparison between the two reveals degree to which sampling is satisfactory. In HDL the two estimates of  $K_T$  agree very well, but in LDL, below the  $K_T$  maximum, the deviations between the two indicate that sampling in LDL is not sufficient to obtain  $K_T$  from fluctuations.

---

[1] Sastry S, Angell CA (2003) Liquid-Liquid phase transition in supercooled silicon. Nature Materials 2:739-743.

- [2] Speedy RJ, Angell CA (1976) Isothermal compressibility of supercooled water and evidence for a thermodynamic singularity at  $-45^{\circ}$ . C. J. Chem. Phys. 65:851858.
- [3] Speedy RJ (1982) Stability-Limit Conjecture. An Interpretation of the Properties of Water J. Phys. Chem. 86:982991.
- [4] Debenedetti PG, D'Antonio MC (1985) On the nature of the tensile instability in metastable liquids and its relationship to density anomalies. J. Chem. Phys. 84:3339-3345.
- [5] Poole PH, Sciortino F, Essmann U, Stanley HE (1992) Phase behaviour of metastable water. Nature 360:324-328.
- [6] Sastry S, Debenedetti PG, Sciortino F, Stanley HE (1996) Singularity-free interpretation of the thermodynamics of supercooled water. Phys. Rev. E. 53:6144-6154.
- [7] Mishima O, Stanley HE (1998) Decompression-induced melting of ice IV and the liquid-liquid transition in water. Nature 392:164-168.
- [8] Liu, Y, Panagiotopoulos AZ, and. Debenedetti, PG (2009) Low-temperature fluid-phase behavior of ST2 water. J. Chem. Phys. 131:104508(1)-104508(7).
- [9] Saika-Voivod I, Sciortino F, Poole PH (2000) Computer simulations of liquid silica: Equation of state and liquid-liquid phase transition. Phys. Rev. E. 63:011202(1)-011202(9).
- [10] Aptekar L I (1979) Phase transitions in noncrystalline germanium and silicon. Soviet Physics Doklady 24:993-995.
- [11] Donovan, E. P., Spaepen, F., Turnbull, D., Poate, J. M. and Jacobson, D. C. Calorimetric studies of crystallisation and relaxation of amorphous Si and Ge prepared by ion implantation. *J. Appl. Phys.* **57**, 1795 – 1804 (1985).
- [12] Deb S K, Wilding M, Somayazulu M, McMillan P F (2001) Pressure-induced amorphization and an amorphous-amorphous transition in densified porous silicon. Nature 414:528-530.
- [13] Hedler A, Klaumünzer S L, Wesch W (2004) Amorphous silicon exhibits a glass transition. Nature Materials 3:804-809.
- [14] Angell CA, Borick S, Grabow M (1996) Glass transitions and first order liquid-metal-to-semiconductor transitions in 456 covalent systems. J. Non-Cryst. Solids 205207:463471.
- [15] Ashwin SS, Waghmare UV, Sastry S (2004) Metal-to-Semimetal Transition in Supercooled Liquid Silicon. Phys. Rev. Lett. 92: 175701.
- [16] Ganesh P, Widom M (2009) Liquid-Liquid Transition in Supercooled Silicon Determined by First-Principles Simulation. Phys Rev Lett 102:075701-1075701-4.

- [17] Kurita R, Murata KI, Tanaka H (2008) Control of fluidity and miscibility of a binary liquid mixture by the liquid-liquid transition. *Nature Materials* 7:647-652.
- [18] Debenedetti PG (2003) Supercooled and glassy water. *J. Phys.: Condens. Matter* 15 R1669R1726.
- [19] Mallamace F, Broccio M, Corsaro C, Faraone A, Majolino D, Venuti V, Liu L, Mou CY, Chen SH (2007) Evidence of the existence of the low-density liquid phase in supercooled, confined water. *Proc. Natl. Acad. Sci. USA* 104:424-428.
- [20] Angell CA (2008) Insights into Phases of Liquid Water from Study of Its Unusual Glass-Forming Properties. *Science* 319:582-587.
- [21] Stillinger FH, Weber TA (1985) Computer simulation of local order in condensed phases of silicon. *Phys. Rev. B.* 32:5262-5171.
- [22] Kim, T H *et al* (2005) *In situ* High-Energy X-Ray Diffraction Study of the Local Structure of Supercooled Liquid Si. *Phys. Rev. Lett.* 95:085501.
- [23] ten Wolde PR, Frenkel D (1997) Enhancement of Protein Crystal Nucleation by Critical Density Fluctuations. *Science* 277: 1975-1978.
- [24] Ghiringhelli LM, Valeriani C, Meijer EJ, Frenkel D (2007) Local Structure of Liquid Carbon Controls Diamond Nucleation. *Phys. Rev. Lett.* 99:055702.
- [25] Voronin G, Pantea C, Zerda T, Wang L, Zhao Y (2003) In situ x-ray diffraction study of silicon at pressures up to 15.5 GPa and temperatures up to 1073 K. *Phys. Rev. B.* 68:020102-1-020102-4.
- [26] Sciortino F, Geiger A, Stanley HE (1991) Network defects and molecular mobility in liquid water. *J. Chem. Phys.* 96:3857-3865.
- [27] Dazhi Liu D *et al* (2007) Observation of the density minimum in deeply supercooled confined water. *Proc. Natl. Acad. Sci (USA)* 104: 95709574.
- [28] Corti DS, Debenedetti PG (1994) A Computational Study of Metastability in Vapor-Liquid Equilibrium. *Chem. Eng. Sci.* 49:2717-2734.
- [29] Saw S, Ellegaard NL, Kob W, Sastry S (2009) Structural Relaxation of a Gel Modeled by Three Body Interactions. *Phys. Rev. Lett.* 103:248305.
- [30] Plimpton S (1995) Fast parallel algorithms for short-range molecular dynamics. *J. Comput. Phys.* 1-19.

# Figure Captions

**Figure 1: Equation of state.** (top panel) Plot of pressure against density isotherms from NPT simulations. Isotherms for  $T \geq 1133K$  are continuous, and the lines through the data points are polynomial fits used to obtain the compressibility. For  $1133K \leq T \leq 1259K$ , the isotherms show an inflection, corresponding to a compressibility maximum. For  $T < 1133K$ , the isotherms show a density discontinuity signaling a first order transition. The crossing of isotherms at positive pressures reflects the presence of density maxima. (bottom panel) Pressure *vs.* density below the critical point from NPT (open symbols) and NVT (filled symbols) simulations. Pressures from NVT simulations below  $T = 1133K$  exhibit non-monotonic behavior at intermediate densities indicating a phase transition, while matching with pressures from NPT simulation at high, low densities. The critical temperature lies between  $T = 1133K$  and  $T = 1108K$ .

**Figure 2: Compressibility maxima increase with decrease in temperature.** Compressibilities  $K_T$  *vs.* pressure for different temperatures from NPT simulations. The lines show  $K_T$  calculated from the derivative of the pressure along isotherms and the symbols show  $K_T$  calculated from volume fluctuations. The maximum value of  $K_T$  increases as temperature decreases, indicating an approach to a critical point.

**Figure 3: Coordination number and Diffusivity.** (top panel) Plot of coordination number  $N_n$  against pressure for different temperatures obtained from NPT simulations. In HDL, the  $N_n$  is around five and in LDL it approaches four, corresponding to tetrahedral local structure. (bottom panel) Plot of diffusivity  $D$  against pressure for different temperatures.  $D$  is calculated from the mean square displacement, and shows a dramatic drop of over two orders of magnitude as the liquid transforms from HDL to LDL.

**Figure 4: Relationship between structure and dynamics.** Plot of diffusivity  $D$  against coordination number  $N_n$  at different temperatures. Lines through the data points are guides to the eye, and highlight the remarkably similar dependence of  $D$  on  $N_n$  at all temperatures including those below the critical temperature where both  $D$  and  $N_n$  change discontinuously. (inset) Plot of  $D$  (scaled to match at  $N_n = 4.8$ ) *vs.*  $N_n$ , showing data collapse. The line is a Vogel-Fulcher-Tammann (VFT) fit, with a vanishing diffusivity = 3.86.

**Figure 5: Phase Diagram in PT plane.** The pressure-temperature phase diagram showing the location of (a) the liquid-crystal phase boundary [25], (b) the liquid-gas phase

boundary and critical point, (c) the liquid-liquid phase boundary and critical point, (d) the liquid spinodal (e) the tensile limit obtained from two different increasing tensile pressure at two different rates, (f) the density maximum (TMD) and minimum (TMinD) lines, and (g) the compressibility maximum (TMC) and minimum (TMinC) line. Lines joining TMD and TMinD (dot-dashed), TMC and TMinC (dashed) are guides to the eye. (inset) Enlargement of box in main panel showing that TMD and spinodal lines do not intersect.

# Figures

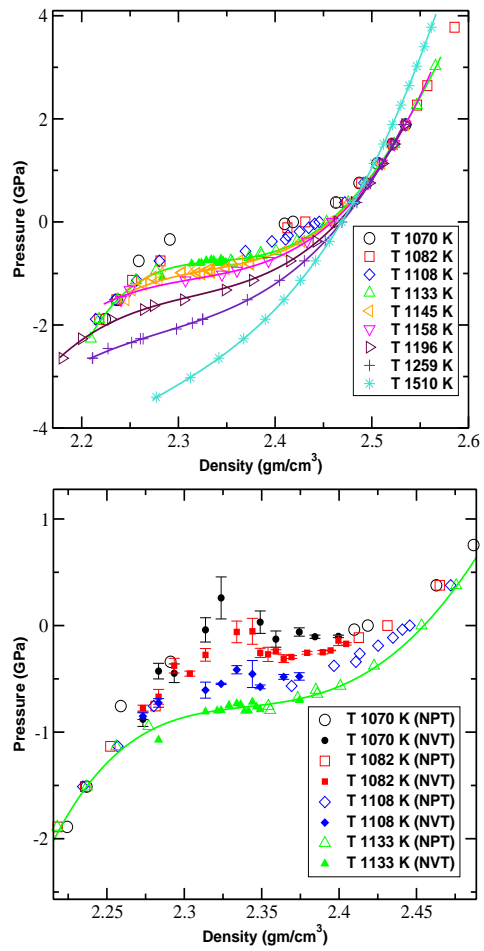


FIG. 1: Vasisht et al

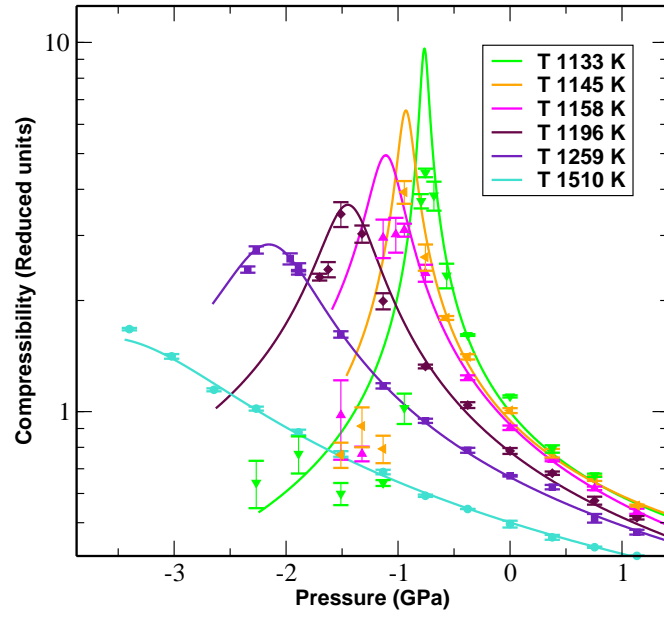


FIG. 2: Vasisht et al

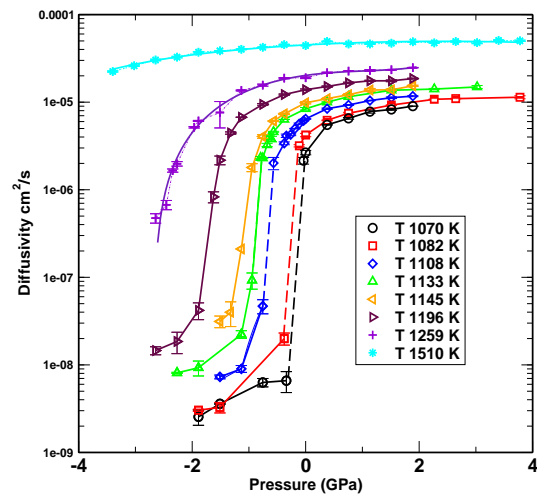
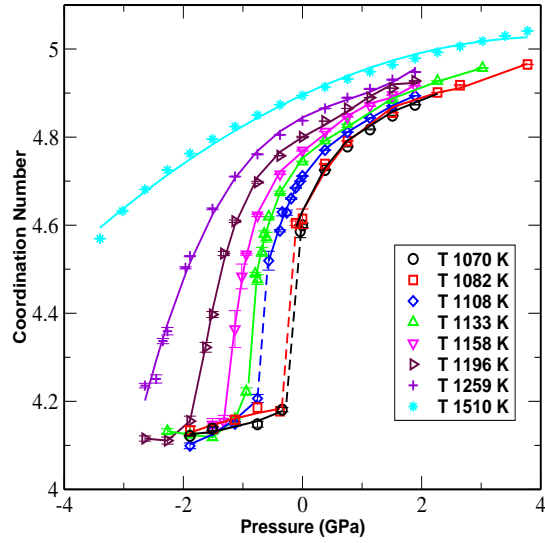


FIG. 3: Vasisht et al

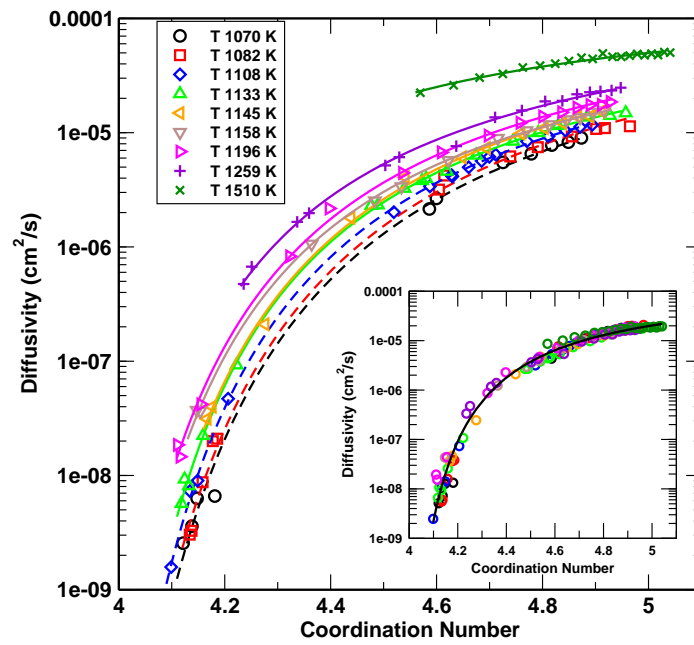


FIG. 4: Vasisht et al

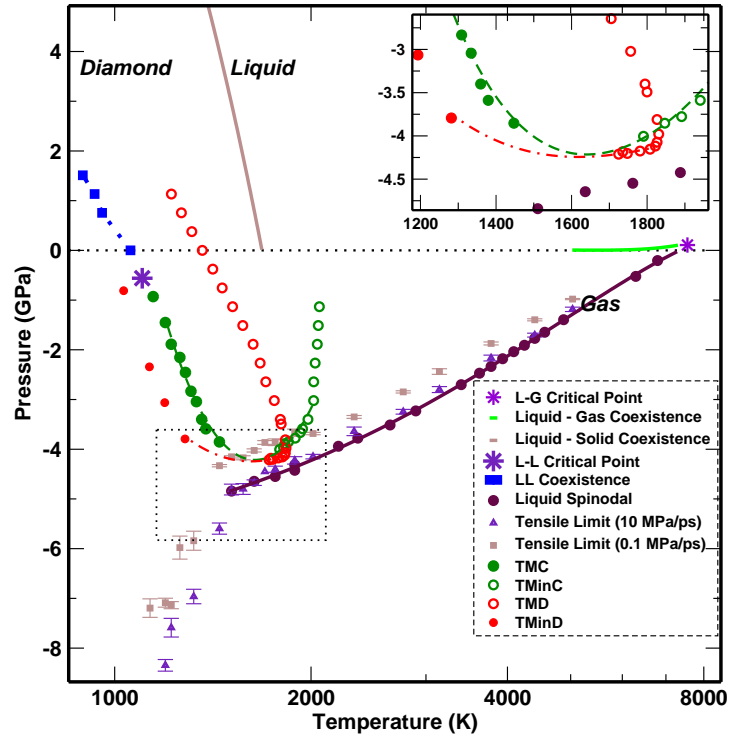


FIG. 5: Vasisht et al